ELSEVIER

Journal of Structural Geology 28 (2006) 1093–1102

JOURNAL OF STRUCTURAL GEOLOGY

www.elsevier.com/locate/jsg

Fracture strength of tourmaline and epidote by three-point bending test: application to microboudin method for estimating absolute magnitude of palaeodifferential stress

Nozomi Kimura [a,*], Hideo Awaji [b], Masato Okamoto [b], Yoshihisa Matsumura [b], Toshiaki Masuda [a]

[a] *Institute of Geosciences, Shizuoka University, Shizuoka 422-8529, Japan*
[b] *Department of Materials Science and Engineering, Nagoya Institute of Technology, Nagoya 466-8555, Japan*

Available online 8 May 2006

Abstract

Three-point bending tests are conducted on millimetre-scale tourmaline and epidote samples at room temperature and pressure to determine fracture strengths suitable for use with the microboudin method of palaeostress analysis. The fracture strength of the samples is obtained from the Weibull scale and shape parameters using a size-effect model. Three different size-effect models are evaluated and it is found that the effective-length model is the most appropriate for describing the fracture strength of tourmaline and epidote based on geological constraints. The palaeodifferential stresses determined by this method for samples from Wadi Tayin (Sultanate of Oman), Greenbushes (Australia) and four high-pressure metamorphic belts in Japan are in the range of 10–300 MPa.

Keywords: Absolute magnitude; Epidote; Fracture strength; Microboudin method; Palaeodifferential stress; Size effect; Three-point bending test; Tourmaline

1. Introduction

Differential stress drives rock deformation and is a key factor in mountain building and plate tectonics. Stress analysis is thus a central theme in structural geology (e.g. Hobbs et al., 1976). Three metallurgical methods of stress analysis using grain size, subgrain size and dislocation density were introduced in the 1970s and later applied to monomineralic metamorphic tectonites to estimate the magnitude of palaeo-differential stress during plastic deformation within orogenic belts (e.g. Mercier et al., 1977; Twiss, 1977; Weathers et al., 1979; Etheridge and Wilkie, 1981; Ord and Christie, 1984). However, these metallurgical methods involve substantial uncertainty due to the requirement of an assumption of steady-state deformation, which is unlikely in orogenic processes (e.g. White et al., 1980; Passchier and Trouw, 2005). The calcite twin and microboudin methods have subsequently been proposed for palaeostress analysis based on the observation of microstructures in deformed rocks (e.g. Jamison and Spang, 1976; Masuda et al., 1989; Rowe and Rutter, 1990; Lacombe, 2001). The calcite twin method is applied to marbles and calcite veins, whereas the microboudin method is applied to quartzose metamorphic tectonites. Both methods are considered to be more suitable than the first metallurgy-based methods as both consider non-steady state deformation.

The microboudin method for palaeostress analysis was proposed by Masuda et al. in 1989 and has been subsequently refined by a number of revisions (Masuda et al., 1990, 2003, 2004a). The method has been successfully applied to microboudinage of columnar minerals such as piemontite, tourmaline and sodic amphibole grains embedded within a quartz matrix in metamorphic tectonites (e.g. Masuda et al., 2003, 2004a,b). The relation determined by the microboudin method is given in terms of a dimensionless stress parameter λ, which is defined as

$$\lambda = \frac{\sigma_0}{S^*} \tag{1}$$

where σ_0 is the far-field differential stress and S^* is the modal extension-fracture strength of columnar mineral grains with unit aspect ratio (see Appendix A for determination of λ by the microboudin method). Thus, if S^* is provided, the microboudin method can give the absolute magnitude of σ_0. However, as direct measurement of S^* for micrometre-scale columnar minerals at metamorphic temperatures and pressures is technically difficult, it remains necessary to determine S^* by alternative means. In this study, three-point bending tests are

* Corresponding author.
E-mail address: r5444002@ipc.shizuoka.ac.jp (N. Kimura).

0191-8141/$ - see front matter © 2006 Elsevier Ltd. All rights reserved.
doi:10.1016/j.jsg.2006.03.020

Nomenclature

λ	dimensionless stress parameter
σ_0	far-field differential stress
S^*	modal extension-fracture strength of columnar minerals (general)
P	measured load at failure
l, b and h	span distance (mm), breadth (mm) and height (mm) of specimen
m	Weibull shape parameter (Weibull modulus)
β_3, β_t	Weibull scale parameter for three-point bending test and tensile test, respectively
S_t	modal fracture strength with the size of (l mm, b mm, b mm)
S_b^*, S_w^*	modal fracture strength for cubes with dimensions b (mm) and w (mm), respectively
V_3, V_t	effective volume for three-point bending test and tensile test, respectively
A_3, A_t	effective area for three-point bending test and tensile test, respectively
L_3, L_t	effective length for three-point bending test and tensile test, respectively

conducted on millimetre-scale tourmaline and epidote at room temperature and pressure and S^* for these minerals is deduced by considering the size effect of fracture strength. Using the values of S^* thus determined and assuming no influence of temperature and pressure on S^*, the magnitude of σ_0 is tentatively estimated for metacherts from various parts of Japan and the Sultanate of Oman and also for a pegmatite from Australia.

2. Three-point bending tests

The three-point bending test (e.g. Davidge, 1979; Awaji, 2001) is the most practical method for determining the fracture strength of columnar minerals due mainly to the simplicity of sample preparation compared with that for other mechanical tests such as the Brazilian test or even the simple tensile test.

2.1. Materials

Of the microboudinaged minerals available in sample rocks, tourmaline and epidote were chosen for testing as the only minerals with crystals of sufficient size for treatment. Tourmaline samples collected from Stak Nala, Gilgit, Pakistan and epidote samples from Warsar, Peshawar, Pakistan were selected for analysis. A total of 13 tourmaline test pieces (span distance, 3 mm; breadth, 1 mm; height, 1 mm) and 10 epidote test pieces (8 mm, 2 mm, 2 mm) were prepared (Fig. 1). The longitudinal side of the test piece was cut parallel to the crystallographic c axis and the test surfaces were carefully polished with diamond paste to remove minute cracks introduced by saw-cut processes.

2.2. Method

The three-point bending test was performed at room temperature and pressure using an Autograph (Shimadzu, Japan) at the Nagoya Institute of Technology. The crosshead speed for this test was set at 0.5 mm/min. The flexural strength, s, is calculated by

$$s = \frac{3Pl}{2bh^2} \tag{2}$$

where P is the measured load at failure and l, b and h are the span distance, breadth and height of the rectangular prism-shaped test pieces, as shown in Fig. 2 (e.g. Davidge, 1979, p. 16).

2.3. Experimental results

Fig. 3 shows Weibull plots of the fracture strengths of tourmaline and epidote obtained in the tests. The strength data vary widely, from 22.2 to 165.9 MPa for tourmaline and from 39.6 to 198.9 MPa for epidote. Representative values of strength are determined by statistical analysis using the

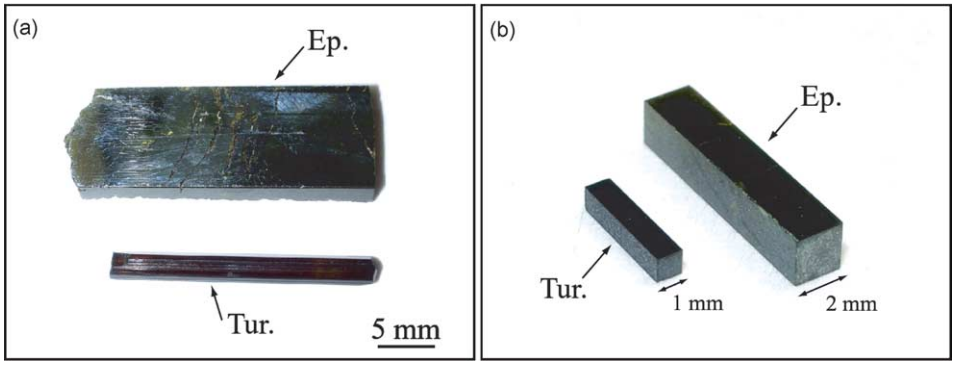

Fig. 1. Photographs of specimens for three-point bending tests. Tur.=tourmaline. Ep.=epidote. (a) Bare blocks of tourmaline and epidote. (b) Test pieces of tourmaline and epidote.

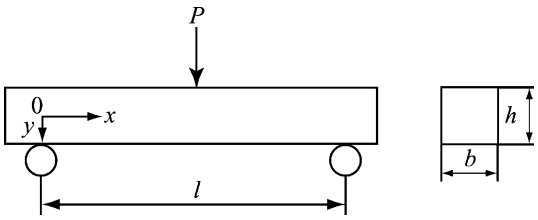

Fig. 2. Schematic illustration of specimen for three-point bending tests.

well-established Weibull theory (e.g. Epstein, 1948; Weibull, 1951). The cumulative distribution function of Weibull theory is given by

$$F(s) = 1 - \exp\left\{-\left(\frac{s}{\beta_3}\right)^m\right\} \tag{3}$$

where s is the strength of failure, m is the shape parameter (Weibull modulus) and β_3 is the scale parameter for three-point bending tests. Here, m and β_3 are representative values called the Weibull parameters: m is a material constant representing the scatter of fracture strength and β_3 is a reference value analogous to a mean or median value of strength dependent on material size. The Weibull parameters determined from the present data by linear regression (e.g. Davidge, 1979, p. 136) are coincidently the same for both tourmaline and epidote: $m=2$ and $\beta_3=110$ MPa. The numbers of the significant figure are judged to be 1 for m and 2 for β_3 from the data for both tourmaline and epidote shown in Fig. 3. The data do not fit well to a straight-line fitting, which is not rare for ceramics with $m<5$ (e.g. Atkinson et al., 2002).

3. Derivation of modal extension-fracture strength S^* from the scale parameter β_3

It should be noted that the value of β_3 obtained above is not equivalent to S^* in Eq. (1). Here, new parameters β_t, S_t and S_b^* are introduced to derive S^* from β_3 in four steps (Fig. 4), where β_t is the Weibull scale parameter for tensile tests, S_t is the modal fracture strength for an identically sized grain and S_b^* is that for cubic mineral grains of dimension b (mm). In all steps,

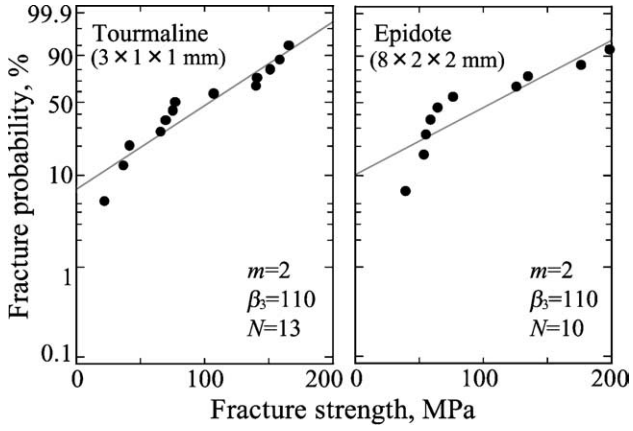

Fig. 3. Weibull plot of fracture strength for tourmaline and epidote. Solid circles denote strength data. The vertical axis is determined by the median lank method (e.g. Davidge, 1979, p.136). N is the number of test pieces.

the size and shape effects of fracture strength are considered in the calculation.

Three size-effect models for fracturing (effective volume, effective area and effective length) have been formulated based on the Weibull theory and the appropriate use of each depends on the site of critical imperfections for fracturing in the specimen. Specifically, the effective-volume model is applicable to cases in which the effective imperfections for fracturing are distributed in the bulk, while the effective-area model is to be adopted when effective imperfections occur on the surface of the test piece (e.g. Davidge, 1979, p. 138; Awaji, 2001). The effective-length model is used when the effective imperfections are distributed on the longitudinal edges of the test piece (Matsuo et al., 1984). As it is not known which model is best suited for the fracturing of tourmaline and epidote, these three models are evaluated in detail below. Treatment of the size effect for fracture strength commences with calculations of the effective volume, area and length for the test pieces (Appendix B).

3.1. Step 1: from β_3 to β_t (Fig. 4a)

The Weibull scale parameter for the three-point bending test (β_3) differs from that for the simple tensile test (β_t) even for test pieces of identical size because the stress distribution in the test piece is not equivalent in the two tests. Assuming the effective-volume model, the relationship between two strengths, S_1 and S_2, determined by the two test modes and the effective volumes, V_1 and V_2, for each mode is given by

$$\frac{s_1}{s_2} = \left(\frac{V_2}{V_1}\right)^{1/m} \tag{4}$$

where m is the Weibull modulus (e.g., Davidge, 1979, p. 139; Awaji, 2001). Thus, the relationship between β_3 and β_t is expressed by

$$\frac{\beta_t}{\beta_3} = \left(\frac{V_3}{V_t}\right)^{1/m} \tag{5}$$

where V_3 and V_t are the effective volumes for the three-point bending test and the tensile test, respectively (e.g. Davidge, 1979, p. 138; Awaji, 2001). V_3 and V_t appear in Eqs. (45) and (48) (see Appendix B). Substituting these equations into Eq. (5) gives

$$\frac{\beta_t}{\beta_3} = \left(\frac{1}{2(m+1)^2}\right)^{1/m} \tag{6}$$

β_t is then given by

$$\beta_t = \left(\frac{1}{2(m+1)^2}\right)^{1/m} \beta_3 \tag{7}$$

Similarly, the effective-area and effective-length models assume

$$\frac{\beta_t}{\beta_3} = \left(\frac{A_3}{A_t}\right)^{1/m} \tag{8}$$

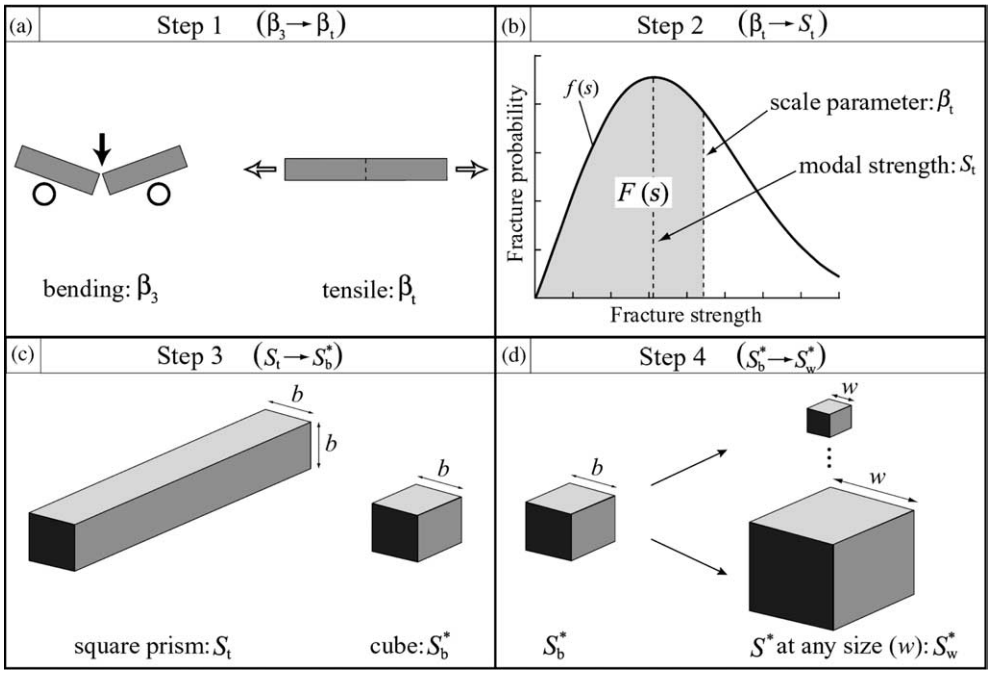

Fig. 4. Schematic illustration of four steps for derivation of S_w^* from β_3. (a) Step 1: from β_3 to β_t. (b) Step 2: from β_t to S_t. (c) Step 3: from S_t to S_b^*. (d) Step 4: from S_b^* to S_w^*.

and

$$\frac{\beta_t}{\beta_3} = \left(\frac{L_3}{L_t}\right)^{1/m} \tag{9}$$

where A_3 and A_t are the effective areas and L_3 and L_t are the effective lengths for the three-point bending test and the tensile test, respectively (e.g. Sutherland et al., 1999; Awaji, 2001). The following common expression can then be derived by substituting Eqs. (46) and (49) and Eqs. (47) and (50) (Appendix B) into Eqs. (8) and (9), respectively:

$$\beta_t = \left(\frac{1}{4(m+1)}\right)^{1/m} \beta_3 \tag{10}$$

3.2. Step 2: from β_t to S_t (Fig. 4b)

The relationship between the Weibull scale parameter for the tensile test (β_t) and the modal tensile fracture strength (S_t) for a specimen of a given size is as follows. The probability density function of the Weibull theory (e.g. Epstein, 1948; Weibull, 1951) is given by

$$f(s) = \frac{m}{\beta_t}\left(\frac{s}{\beta_t}\right)^{m-1} \exp\left\{-\left(\frac{s}{\beta_t}\right)^m\right\} \tag{11}$$

S_t satisfies the relation

$$\frac{df(s)}{ds} = 0 \tag{12}$$

Finally, Eq. (12) gives S_t as follows

$$S_t = \beta_t\left(\frac{m-1}{m}\right)^{1/m} \tag{13}$$

3.3. Step 3: from S_t to S_b^* (Fig. 4c)

S_b^* is defined as the modal fracture strength of a cube with dimension b (mm). From Eq. (4), the relationship between S_t and S_b^* for the effective-volume model is given by

$$\frac{S_b^*}{S_t} = \left(\frac{V_t}{V_b}\right)^{1/m} = \left(\frac{l \times b \times b}{b \times b \times b}\right)^{1/m} \tag{14}$$

where V_t and V_b are the effective volume for the tensile strength S_t and S_b^*, respectively. In this case, V_t is shown in Eq. (48) and V_b corresponds to Eq. (48) with $l=b$. The expressions obtained for the effective-area and effective-length models are

$$\frac{S_b^*}{S_t} = \left(\frac{A_t}{A_b}\right)^{1/m} = \left(\frac{4 \times l \times b}{4 \times b \times b}\right)^{1/m} \tag{15}$$

and

$$\frac{S_b^*}{S_t} = \left(\frac{L_t}{L_b}\right)^{1/m} = \left(\frac{4 \times l}{4 \times b}\right)^{1/m} \tag{16}$$

where A_t and A_b are the effective area and L_t and L_b are the effective length corresponding to the tensile strength S_t and S_b^*, respectively. In this case, A_t and L_t are shown in Eqs. (49) and (50) and A_b and L_b correspond to Eqs. (49) and (50) with $l=b$, respectively. Thus, all three models give the same expression:

$$S_b^* = S_t \times r^{1/m} \tag{17}$$

where r is the aspect ratio given by l/b.

3.4. Step 4: from S_b^* to S_w^* (Fig. 4d)

S^* is the modal tensile-fracture strength of a cube and that for cubes of dimension b or w (mm) are designated S_b^* or S_w^*.

The relationships between S_b^* and S_w^* are expressed as

$$\frac{S_w^*}{S_b^*} = \left(\frac{V_b}{V_w}\right)^{1/m} \tag{18}$$

$$\frac{S_w^*}{S_b^*} = \left(\frac{A_b}{A_w}\right)^{1/m} \tag{19}$$

and

$$\frac{S_w^*}{S_b^*} = \left(\frac{L_b}{L_w}\right)^{1/m} \tag{20}$$

for the effective-volume, effective-area and effective-length models, respectively. V_w is the effective volume, A_w is the effective area and L_w is the effective length corresponding to the tensile strength S_w^*. In this case, V_w corresponds to Eq. (48) with $b=l=w$. Thus, $V_w=w^3$. Similarly, $A_w=4w^2$ are obtained from Eq. (49) and $L_w=4w$ are obtained from Eq. (50). Eqs. (18)–(20) can thus be rewritten as

$$\frac{S_w^*}{S_b^*} = \left(\frac{b^3}{w^3}\right)^{1/m} \tag{21}$$

$$\frac{S_w^*}{S_b^*} = \left(\frac{b^2}{w^2}\right)^{1/m} \tag{22}$$

and

$$\frac{S_w^*}{S_b^*} = \left(\frac{b}{w}\right)^{1/m} \tag{23}$$

where b is the breadth of the test piece in the three-point bending test and w is the width of the fibre that forms the microboudinage structure. As can be seen from the behaviour of S_b^* and S_w^*, the value of S^* in Eq. (1) changes according to the size of the microboudin.

3.5. Summary of derivation

The final equations for S^*, expressed as a function of $w(S_w^*)$ for the effective-volume, effective-area and effective-length models, are

$$S_w^* = \beta_3 \left(\frac{b^3}{w^3}\right)^{1/m} r^{1/m} \left(\frac{m-1}{m}\right)^{1/m} \left(\frac{1}{2(m+1)^2}\right)^{1/m} \tag{24}$$

$$S_w^* = \beta_3 \left(\frac{b^2}{w^2}\right)^{1/m} r^{1/m} \left(\frac{m-1}{m}\right)^{1/m} \left(\frac{1}{4(m+1)}\right)^{1/m} \tag{25}$$

and

$$S_w^* = \beta_3 \left(\frac{b}{w}\right)^{1/m} r^{1/m} \left(\frac{m-1}{m}\right)^{1/m} \left(\frac{1}{4(m+1)}\right)^{1/m} \tag{26}$$

where $b=1$ mm, $r=3$, $m=2$ and $\beta_3=110$ MPa for tourmaline and $b=2$ mm, $r=4$, $m=2$ and $\beta_3=110$ MPa for epidote. These equations can be rewritten in the following form:

$$S_w^* = 32 \times \left(\frac{1}{w^3}\right)^{1/2} \tag{27}$$

$$S_w^* = 39 \times \left(\frac{1}{w^2}\right)^{1/2} \tag{28}$$

$$S_w^* = 39 \times \left(\frac{1}{w}\right)^{1/2} \tag{29}$$

for tourmaline and

$$S_w^* = 100 \times \left(\frac{1}{w^3}\right)^{1/2} \tag{30}$$

$$S_w^* = 90 \times \left(\frac{1}{w^2}\right)^{1/2} \tag{31}$$

$$S_w^* = 64 \times \left(\frac{1}{w}\right)^{1/2} \tag{32}$$

for epidote.

4. Estimation of far-field differential stress σ_0 from microboudinage structures

The above results (Eqs. (27)–(32)) are applied to tourmaline microboudinage structures embedded within quartzose matrices from the Wadi Tayin (Oman) and Greenbushes (Australia) samples and to piemontite (Mn-rich epidote) from four high P–T metamorphic rocks from Japan (Table 1). The Greenbushes sample is a pegmatite, while the other samples are metacherts. These six samples are the same as those analysed

Table 1
The obtained values of far-field differential stress (σ_0) and other essential data for each sample.

Sample	Mineral	Mean width (mm)	λ	Far-field differential stress (σ_0)			Tectonic setting	Pressure at $T=300$ °C (MPa)
				Effective-length (MPa)	Effective-surface (MPa)	Effective-volume (MPa)		
Wadi Tayin	Tur.	0.019	0.42	120	860	5100	Metamorphic sole	200–400
Greenbushes	Tur.	5.2	0.68	12	5.1	1.8	Pegmatite	350–500
Nuporomaporo	Pi.	0.029	0.77	290	2400	16000	High P region	ca. 300
Yamagami	Pi.	0.019	0.51	240	2400	20000	High P region	ca. 300
Matsunosako	Pi.	0.057	0.32	86	510	2400	High P region	ca. 300
Asemi	Pi.	0.036	0.14	47	350	2000	High P region	ca. 300

by Masuda et al. (1989, 2003), where the geological settings have been summarised.

As S^* in Eq. (1) is replaced by S_w^*, the far-field differential stress (σ_0) can be calculated by

$$\sigma_0 = \lambda S_w^* \tag{33}$$

4.1. Dimensionless stress parameter λ

The determination of λ is performed by employing experimentally determined $m=2$ for both piemontite and tourmaline. The method for obtaining λ is outlined briefly in Appendix A. The results are shown in Fig. 5 and Table 1. The values of λ obtained in this study for piemontite are the same as those obtained in previous analyses of piemontite microboudins, which were also performed using $m=2$ (Masuda et al., 2003). However, as the previous determination for tourmaline was performed with $m=4$, the present values differ slightly.

4.2. Modal extension-fracture strength S_w^*

As the fracturing to form microboudinaged grains occurred at high pressure and temperature, the influence of these conditions on S_w^* should be critical. However, for the sake of simplicity, the influences of these conditions are initially assumed to be negligible and will be discussed later.

The size effect is critical in the estimation of S_w^*, which is ignored in the previous microboudin analysis of Masuda et al. (e.g. Masuda et al., 2003, 2004a,b). The grain size of piemontite and tourmaline varies from grain to grain. As the grain-size distributions of all the analysed samples are log-normal (Fig. 6), the geometric mean grain size ($\bar{w}$) is used for the analysis (Table 1). The S_w^* values are properly calculated using Eqs. (27)–(32).

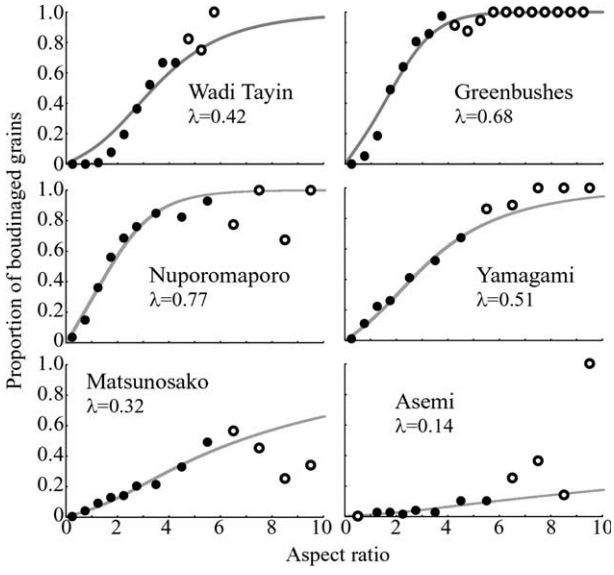

Fig. 5. Results of the microboudin method for the present samples. Solid and open circles denote reliable and unreliable data (>25 measured grains are regarded as reliable). The curve represents the best-fit $G(r,\lambda)$ using reliable data. The obtained values of λ for each sample are indicated.

4.3. Far-field differential stress σ_0

The magnitude of σ_0 is calculated separately using Eq. (33) through substitution of λ and S_w^* for the three size-effect models and for tourmaline and epitode. Table 1 summarises the tentative values of σ_0 obtained for the six samples. Note that the σ_0 values of the Greenbushes samples under the effective-volume model are smaller than those for the effective surface and length models, attributable to the large mean grain size of tourmaline (>1 mm).

5. Evaluation of size-effect models based on geological constraints

In the list of obtained palaeodifferential stresses in Table 1, extraordinarily large estimates such as 20000 and 16000 MPa are seen, which are of course impossible conditions in nature. To evaluate these inappropriate estimates and eliminate unsuitable size-effect models for the analysis of tourmaline and epidote, the level of differential stress in orogenic belts is considered as a geological constraint. Existing differential-stress estimates are also briefly reviewed as a rough guide for the evaluation.

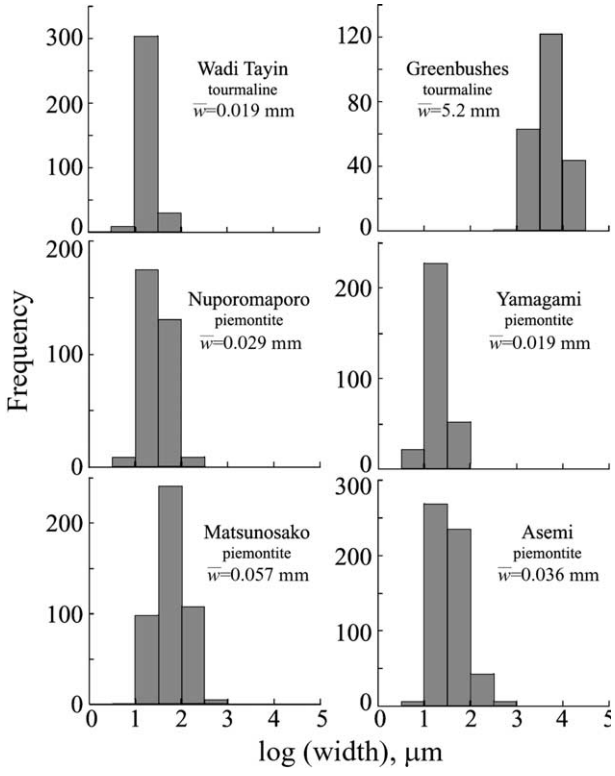

Fig. 6. Frequency distribution of grain width on a logarithmic scale. The geometric mean width ($\bar{w}$) is indicated.

5.1. Ultimate value of far-field differential stress σ_0

The metamorphic pressure (p) and far-field differential stress are related as follows:

$$p = \frac{1}{3}(\sigma_1 + \sigma_2 + \sigma_3) \tag{34}$$

$$\sigma_0 = \sigma_1 - \sigma_3 \tag{35}$$

where, σ_1, σ_2 and σ_3 are the principal stresses ($\sigma_1 \geq \sigma_2 \geq \sigma_3$). From these equations, the following expression can be easily derived:

$$3p = \sigma_0 + \sigma_2 + 2\sigma_3 \tag{36}$$

As $\sigma_2 > 0$ and $\sigma_3 > 0$ are satisfied, it follows that

$$3p > \sigma_0 \tag{37}$$

This represents the ultimate limit of σ_0 that can be generated in the crust.

Microboudinage in metamorphic tectonites occurs during retrograde metamorphism and the microboudinage structures are frozen at 250–300 °C, corresponding to the plastic–brittle transition temperature of matrix quartz (e.g. Masuda et al., 2004b). As petrological studies have shown that the pressures at 250–300 °C for these six samples fall in the range of 200–500 MPa (e.g. Otsuki and Banno, 1990; Partington, 1990; Maruyama et al., 1996; Hacker and Gnos, 1997), Eq. (37) indicates that σ_0 must be lower than 1500 MPa.

5.2. Estimates of differential stress

There are many estimates of differential stress, deviatoric stress and shear stress. Etheridge (1983) concluded, based on occurrences of tensile fracturing of metamorphic rocks, that differential stress intensities during crustal orogenesis would be less than 40 MPa. Hacker (1991) implied in his thermo-mechanical studies of the Oman ophiolite that deformation within the metamorphic sole should have occurred at maximum shear stresses of ~100 MPa, which is similar to the shear stresses estimated by Molnar and England (1990) for thrusting along the Main Central Thrust in the Himalayas. Turcotte and Schubert (2002), based on force balance for the continental block, gives values of deviatoric stress of the order of 10–100 MPa. Sandiford et al. (1995) argued, on torque balance in the Himalayan range, that the differential stress in that region is 45–70 MPa. Profiles of rock strength with respect to depth in the lithosphere based on the mechanical and rheological properties of rocks provide an upper limit for differential stress of 100–1000 MPa depending on the geothermal gradient (e.g. Twiss and Moores, 1992). Many other estimates of differential stress (e.g. metallurgy-based palaeopiezometric studies, calcite-twin studies, in-situ stress measurements, earthquake focal mechanisms, finite element techniques) appear to fall within the order of 10–100 MPa (e.g. Hanks and Raleigh, 1980; Research Group of Heidelberg Academy of Sciences and Humanities, 2004).

5.3. Evaluation of size-effect models

Table 1 summarises the differential stress determined by the three size-effect models for each sample. Assuming that the size-effect model is not dependent on the mineral species or sample area, the effective-volume and effective-area models yield values for σ_0 that far exceed the geological constraints cited above and are thus unlikely to be applicable for tourmaline and epidote. The effective-length model, however, affords acceptable values of differential stress for all samples. Consequently, the values of σ_0 determined by the microboudin method are 120 MPa for the Wadi Tayin (Sultanate of Oman) sample, 12 MPa for the Greenbushes (Australia) sample, 290 MPa for the Nuporomaporo (Northern Japan) sample, 240 MPa for the Yamagami (Northeast Japan) sample, 86 MPa for the Matsunosako (Southern Japan) sample and 47 MPa for the Asemi (Southwest Japan) sample.

6. Discussion

The derived values of S_w^* for tourmaline and epidote are essentially only valid at room temperature and pressure. As microboudinage in metamorphic tectonites occurs at much higher temperature and pressure, the influence of pressure–temperature variations on S_w^* should be evaluated. Residence time should also be considered, as longer periods under high pressure–temperature conditions can promote the degradation of fracture strength. This has been observed directly for ceramics (e.g. Davidge, 1979; Lawn, 1993). Although the influence of these factors on fracture strength has been studied with respect to polycrystalline rocks such as granite, marble and gabbro, no such attempt has been made for single crystals. Here, the effects of temperature, pressure and time on the fracture strength of tourmaline and epidote are evaluated with reference to previous studies on polycrystalline rocks.

6.1. Temperature

The dependence of the fracture strength of polycrystalline rocks on temperature is considered to be small up to 600 °C (e.g. Davidge, 1979, p. 17; Shimada, 1993; Lenz et al., 2002; Rocchi et al., 2004; Paterson and Wong, 2005, p. 28). Ceramics are generally considered to be heat-resistant materials, maintaining strength to temperatures as high as 600 °C (e.g. Sowden et al., 1974; Quispe-Cancapa et al., 2005; Eskner and Sandström, in press). As tourmaline and epidote are silicate minerals and can be considered a type of ceramic, the fracture strength of tourmaline and epidote are considered to exhibit negligible dependence on temperature, although there is a lack of such data to confirm this consideration.

6.2. Pressure

Experiments on polycrystalline rocks have revealed that the fracture strength increases with confining pressure (e.g. Paterson, 1958; Byerlee, 1967, 1968; Rosengren and Jaeger, 1968; Mogi, 1974; Paterson and Wong, 2005, pp. 24–25). For

example, the fracture strengths of granite and gabbro (e.g. Paterson, 1958; Byerlee, 1967; Kranz, 1980; Shimada, 1981, 1993) differ by factors of 1.5 and 2 between confining pressures of 200 and 500 MPa, corresponding to the metamorphic pressure range of the present samples. However, the dependence of strength on pressure has been suggested to be due mainly to the effect of cracks along grain boundaries or joints (e.g. Mogi, 1974; Kranz, 1980; Zoback et al., 2003). As single-crystalline materials such as the tourmaline and epidote samples examined in this study have no grain boundaries or joints, it is considered that the fracture strength of the present samples will vary only marginally with pressure.

6.3. Time

Time is the most difficult parameter to consider with respect to the fracture strength of crystalline minerals because the geological timescale for microboudinage is so much longer than the timescale for the bending test (a few minutes for failure in the present study). It is known that materials undergo time-dependent crack growth at stresses much less than their critical stress and slow crack growth gives rise to static fatigue through chemical reaction between the solid phase and corrosive fluid phases at the crack tip (e.g. Atkinson, 1987; Lawn, 1993; Paterson and Wong, 2005). For instance, Wilkins (1980) experimentally measured time to failure under subcritical stresses for a granite and revealed that average crack-growth velocities are as low as 10^{-12} m/s. Lankford (1987, 1989) quantitatively links the fracture strength of ceramics with the applied strain rate and explains his observations in terms of sub-critical crack growth by the mechanism of stress corrosion. Others have also demonstrated this type of time-dependent failure strength for ceramics and polycrystalline rocks: most fracture at 40–80% of the critical stress when loaded for longer than 10^5 s (e.g. Baker and Preston, 1946; Anderson and Grew, 1977; Lajtai et al., 1987; Gong and Du, 2000; Takahashi et al., 2005). As the degradation of strength with time is typical for oxide ceramics (e.g. Davidge, 1979, p. 139; Lawn, 1993, p. 123; Awaji, 2001, p. 71), it is considered that tourmaline and epidote will undergo a similar process.

6.4. Effect of temperature, pressure and time on modal extension-fracture strength S_w^*

Higher confining pressure tends to increase the absolute value of S_w^*, while increasing residence time tends to reduce S_w^*. The true value of S_w^* under metamorphic conditions will thus be influenced by both effects and is likely to differ from that determined by the three-point bending test at room temperature and pressure. However, the difference is considered to be less than an order of magnitude and the listed σ_0 values are probably acceptable as a first approximation. More realistic estimations of σ_0 in the future will depend on realistic revision of S_w^* to account for geological conditions.

Acknowledgements

The authors thank Y. Yamaura and T. Shibutani for metachert samples, T. Hashida, N. Niitsuma and M.K. Satish for encouragement and H. Mori for the preparation of thin sections. The authors also thank T. Blenkinsop, M.S. Paterson and an anonymous reviewer for constructive comments on the manuscript. This study was supported in part by the Japan Society for the Promotion of Science.

Appendix A. Determination of dimensionless stress parameter λ

The microboudin method consists of two parts: measurement of the proportion of boudinaged grains with respect to aspect ratio ($M(r)$), and theoretical prediction of the proportion as a function of the far-field differential stress (σ_0). $M(r)$ is determined by intensive measurement of the length and width of boudinaged and intact fibre grains with the help of strain reversal method by Ferguson (1981).

The theoretical prediction is derived from the shear-lag model for stress transfer from the matrix to the fibre (e.g. Zhao and Ji, 1997), the weakest-link theory of fracturing (e.g. Weibull, 1951) and the Weibull distribution of fracture strength (e.g. Epstein, 1948). The proportion is given by $G(r,\lambda)$, which is a function of the aspect ratio (r), the Weibull modulus (m) and the dimensionless stress parameter (λ), as follows.

$$G(r,\lambda) = 1-\exp\left[-\frac{m-1}{m}r\lambda^m\left(\frac{E_f}{E_q}\right)^m\left\{1-\left(1-\frac{E_q}{E_f}\right)\frac{1}{\cosh(Ar)}\right\}^m\right] \tag{38}$$

where E_f and E_q are the elastic constants of the fibre and matrix and A_0 is a constant (for details on derivation of these equations, see Masuda et al. (1989, 2003)). The constants E_f/E_q and A_0 for tourmaline fibre and quartz matrix are 2.0 and 0.4 and for piemontite fibre and quartz matrix are 1.5 and 0.5, respectively. The data book by Simmons and Wang (1971) was consulted to obtain these values.

Comparison between $M(r)$ and $G(r,\lambda)$ is the focus of the microboudin method. The value of λ is determined so as to minimise the square difference, $T(\lambda)$, which is defined by

$$T(\lambda) = \sum_r [G(r,\lambda) - M(r)]^2 \tag{39}$$

Appendix B. Effective volume, area and length

The effective volume (V_e), effective area (A_e) and effective length (L_e) can be calculated by

$$V_e = \int_V \left(\frac{s}{s_m}\right)^m dV \tag{40}$$

$$A_e = \int_A \left(\frac{s}{s_m}\right)^m dA \tag{41}$$

and

$$L_e = \int_L \left(\frac{s}{s_m}\right)^m dL \tag{42}$$

where s is the stress at a specific point in the test piece and s_m is the maximum tensile stress applied to the test piece (e.g. Davidge, 1979; Matsuo et al., 1984; Sutherland et al., 1999; Awaji, 2001). Tensile stress is taken as positive only in Appendix B. The values of s and s_m for the three-point bending test are given as

$$s = \frac{6Pxy}{bh^3} \tag{43}$$

and

$$s_m = \frac{3Pl}{2bh^2} \tag{44}$$

where x and y are the Cartesian coordinates, P is the load at failure, b is the breadth, h is the height and l is the span distance (Fig. 2). In this case, $h=b$. The effective volume, area and length for the three-point bending test (V_3, A_3 and L_3) are calculated by substitution of Eqs. (43) and (44) into Eqs. (40)–(42), as follows.

$$V_3 = \int_0^b \int_0^{\frac{h}{2}} \int_0^l \left(\frac{s}{s_m}\right)^m dx dy dz = 2b \int_0^{\frac{h}{2}} \int_0^{\frac{l}{2}} \left(\frac{4xy}{lh}\right)^m dx dy$$

$$= \frac{lbh}{2(m+1)^2} = \frac{lb^2}{2(m+1)^2} \tag{45}$$

$$A_3 = \int_0^b \int_0^l \left(\frac{s}{s_m}\right)^m dx dz = 2b \int_0^{\frac{l}{2}} \left(\frac{2x}{l}\right)^m dx = \frac{lb}{(m+1)} \tag{46}$$

$$L_3 = \int_0^l \left(\frac{s}{s_m}\right)^m dx = 2 \int_0^{\frac{l}{2}} \left(\frac{2x}{l}\right)^m dx = \frac{l}{(m+1)} \tag{47}$$

The effective volume, area and length for the simple tensile test (V_t, A_t and L_t) are given below as equivalent to the volume, area and length of the test piece considering the uniformity of the stress distribution (i.e. $s_m = s$).

$$V_t = lb^2 \tag{48}$$

$$A_t = 4lb \tag{49}$$

$$L_t = 4l \tag{50}$$

References

Anderson, O.L., Grew, P.C., 1977. Stress corrosion theory of crack propagation with applications to geophysics. Reviews of Geophysics and Space Physics 15, 77–104.

Atkinson, B.K., 1987. Fracture Mechanics of Rock. Academic Press, London.

Atkinson, K., Whiter, J.T., Smith, P.A., Mulheron, M., 2002. Failure of small diameter cast iron pipes. Urban Water 4, 263–271.

Awaji, H., 2001. Strength of Ceramic Materials. Corona Publishing, Tokyo (in Japanese).

Baker, T.C., Preston, F.W., 1946. Fatigue of glass under static loads. Journal of Applied Physics 17, 170–178.

Byerlee, J.D., 1967. Frictional characteristics of granite under high confining pressure. Journal of Geophysical Research 72, 3639–3648.

Byerlee, J.D., 1968. Brittle–ductile transition in rocks. Journal of Geophysical Research 73, 4741–4750.

Davidge, R.W., 1979. Mechanical Behavior of Ceramics. Cambridge University Press, Cambridge.

Epstein, B., 1948. Statistical aspects of fracture problems. Journal of Applied Physics 19, 140–147.

Eskner, M., Sandström, R., 2006. Mechanical properties and temperature dependence of an air plasma-sprayed NiCoCrAlY bondcoat. Surface and Coatings Technology 200, 2695–2703.

Etheridge, M.A., 1983. Differential stress magnitudes during regional deformation and metamorphism: upper bound imposed by tensile fracturing. Geology 11, 231–234.

Etheridge, M.A., Wilkie, J.C., 1981. An assessment of dynamically recrystallized grain size as a palaeopiezometer in quartz-bearing mylonite zones. Tectonophysics 78, 475–508.

Ferguson, C.C., 1981. A strain reversal method for estimating extension from fragmented rigid inclusions. Tectonophysics 79, T43–T52.

Gong, J., Du, C., 2000. Environmental effects on the room-temperature static fatigue behaviour of polycrystalline mullite. Materials Science and Engineering A283, 76–81.

Hacker, B.R., 1991. The role of deformation in the formation of metamorphic gradients: ridge subduction beneath the Oman ophiolite. Tectonics 10, 455–473.

Hacker, B.R., Gnos, E., 1997. The conundrum of samail: explaining the metamorphic history. Tectonophysics 279, 215–226.

Hanks, T.C., Raleigh, C.B., 1980. The conference on magnitude of deviatoric stresses in the Earth's crust and uppermost mantle. Journal of Geophysical Research 85, 6083–6085.

Hobbs, B.E., Means, W.D., Williams, P.F., 1976. An Outline of Structural Geology. Wiley, New York.

Jamison, W.R., Spang, J.H., 1976. Use of calcite twin lamellae to infer differential stress. Geological Society of America Bulletin 87, 868–872.

Kranz, L.R., 1980. The effects of confining pressure and stress difference on static fatigue of granite. Journal of Geophysical Research 85, 1854–1866.

Lacombe, O., 2001. Paleostress magnitudes associated with development of mountain belts: insights from tectonic analyses of calcite twins in the Taiwan Foothills. Tectonics 20, 834–849.

Lajtai, E.Z., Schmidtke, R.H., Bielus, L.P., 1987. The effect of water on the time-dependent deformation and fracture of a granite. International Journal of Rock Mechanics and Mining Science & Geomechanical Abstract 24, 247–255.

Lankford, J., 1987. Temperature, strain rate and fibre orientation effects in the compressive fracture of SiC fibre-reinforced glass-matrix composites. Composites 18, 145–152.

Lankford, J., 1989. Dynamic compressive fracture in fiber-reinforced ceramic matrix composites. Materials Science and Engineering A107, 261–268.

Lawn, B.R., 1993. Fracture of Brittle Solids. Cambridge University Press, Cambridge.

Lenz, J., Thies, M., Wollwage, P., Schweizerhof, K., 2002. A note on the temperature dependence of the flexural strength of a porcelain. Dental Materials 18, 558–560.

Maruyama, S., Liou, J.G., Terabayashi, M., 1996. Blueschists and eclogites of the world and their exhumation. Economic Geology 38, 485–594.

Masuda, T., Shibutani, T., Igarashi, T., Kuriyama, M., 1989. Microboudin structure of piemontite in quartz schists: a proposal for a new indicator of relative palaeodifferential stress. Tectonophysics 163, 169–180.

Masuda, T., Shibutani, T., Kuriyama, M., Igarashi, T., 1990. Development of microboudinage: an estimate of changing differential stress with increasing strain. Tectonophysics 178, 379–387.

Masuda, T., Kimura, N., Hara, Y., 2003. Progress in microboudin method for palaeo-stress analysis of metamorphic tectonites: application of mathematically refined expression. Tectonophysics 364, 1–8.

Masuda, T., Kimura, N., Fu, B., Li, X., 2004a. Validity of the microboudin method for palaeo-stress analysis of metamorphic tectonites: application to extraordinarily long sodic amphibole grains in a metachert from Aksu. China. Journal of Structural Geology 26, 203–206.

Masuda, T., Nakayama, S., Kimura, N., Onodera, K., Okamoto, A., 2004b. Triaxial stress state deep in orogenic belts: an example from Turkey. Journal of Structural Geology 26, 2203–2209.

Matsuo, Y., Nagai, F., Sueyoshi, K., 1984. The bending test of ceramics and the statistical analysis for fracturing. Journal of Japan Society of Mechanical Engineers 50, 1894–1899 (in Japanese).

Mercier, J.-C.C., Anderson, D.A., Carter, N.L., 1977. Stress in the lithosphere: inferences from steady state flow of rocks. Pure and Applied Geophysics 115, 199–226.

Mogi, K., 1974. On the pressure dependence of strength of rocks and the coulomb fracture criterion. Tectonophysics 21, 273–285.

Molnar, P., England, P., 1990. Temperatures, heat flux, and frictional stress near major thrust faults. Journal of Geophysical Research 95, 4833–4856.

Ord, A., Christie, J.M., 1984. Flow stresses from microstructures in mylonitic quartzites of the Moine Thrust Zone, Assynt area, Scotland. Journal of Structural Geology 6, 639–654.

Otsuki, M., Banno, S., 1990. Prograde and retrograde metamorphism of hematite-bearing basic schists in the Sanbagawa belt in central Shikoku. Journal of Metamorphic Geology 8, 425–439.

Partington, G.A., 1990. Environmental and structural controls on the intrusion of the giant rare metal Greenbushes pegmatite, Western Australia. Economic Geology 85, 437–456.

Passchier, C.W., Trouw, R.A.J., 2005. Microtectonics, 2nd ed Springer-Verlag, Berlin.

Paterson, M.S., 1958. Experimental deformation and faulting in Wombeyan marble. Geological Society of America Bulletin 69, 465–475.

Paterson, M.S., Wong, T., 2005. Experimental Rock Deformation—The Brittle Field, 2nd ed Springer-Verlag, Berlin.

Quispe-Cancapa, J.J., de Arellano-López, A.R., Martínez-Fernández, J., Sayir, A., 2005. Tensile strength of directionally solidified chromia-doped sapphire. Journal of the European Ceramic Society 25, 1259–1268.

Research Group of Heidelberg Academy of Sciences and Humanities, 2004. World Stress Map Project: http://www.world-stress-map.org/.

Rocchi, V., Sammonds, P.R., Kilburn, C.R.J., 2004. Fracturing of Etnean and Vesuvian rocks at high temperatures and low pressures. Journal of Volcanology and Geothermal Research 132, 137–157.

Rosengren, K.J., Jaeger, J.C., 1968. The mechanical properties of an interlocked low-porosity aggregate. Geotechniques 18, 317–326.

Rowe, K.J., Rutter, E.H., 1990. Paleostress estimation using calcite twinning: experimental calibration and application to nature. Journal of Structural Geology 12, 1–17.

Sandiford, M., Coblentz, D.D., Richardson, R.M., 1995. Ridge torques and continental collision in the Indian–Australian plate. Geology 23, 653–656.

Shimada, M., 1981. The method of compression test under high pressures in a cubic press and the strength of granite. Tectonophysics 72, 343–357.

Shimada, M., 1993. Lithosphere strength inferred from fracture strength of rocks at high confining pressures and temperatures. Tectonophysics 217, 55–64.

Simmons, G., Wang, H., 1971. Single Crystal Elastic Constants and Calculated Aggregate Properties: A Handbook. MIT Press, Cambridge. 370pp.

Sowden, R.G., Antill, J.E., Livey, D.T., Wilks, R.S., 1974. High temperature materials for heat exchangers in nuclear process heat plants. Proceedings of the International Conference Organized by the British Nuclear Energy Society, London, 44.1–44.10.

Sutherland, L.S., Shenoi, R.A., Lewis, S.M., 1999. Size and scale effects in composites: literature review. Composite Science and Technology 59, 209–220.

Takahashi, K., Murase, H., Yoshida, S., Houjou, K., Ando, K., Saito, S., 2005. Improvement of static fatigue strength of Si_3N_4/SiC crack-healed under cyclic stress. Journal of European Ceramic Society 25, 1953–1959.

Turcotte, D.L., Schubert, G., 2002. Geodynamics, 2nd ed Cambridge University Press, Cambridge.

Twiss, R.J., 1977. Theory and applicability of a recrystallized grain size palaeopiezometer. Pure and Applied Geophysics 115, 227–244.

Twiss, R.J., Moores, E.M., 1992. Structural Geology. Freeman and Company, New York.

Weathers, M.S., Bird, J.M., Cooper, R.F., Kohlstedt, D.L., 1979. Differential stress determined from deformation-induced microstructures of the Moine Thrust Zone. Journal of Geophysical Research 84, 7495–7509.

Weibull, W., 1951. A statistical distribution function of wide applicability. Journal of Applied Mechanics 22, 293–297.

White, S.H., Burrows, S.E., Carreras, J., Shaw, N.D., Humphreys, F.J., 1980. On mylonites in ductile shear zones. Journal of Structural Geology 2, 175–187.

Wilkins, B.J.S., 1980. Slow crack growth and delayed failure of granite. International Journal of Rock Mechanics and Mining Sciences & Geomechanics Abstract 17, 365–369.

Zhao, P., Ji, S., 1997. Refinements of shear-lag model and its applications. Tectonophysics 279, 37–53.

Zoback, M.D., Barton, C.A., Brudy, M., Castillo, D.A., Finkbeiner, T., Grollimund, B.R., Moos, D.B., Peska, P., Ward, C.D., Wiprut, D.J., 2003. Determination of stress orientation and magnitude in deep wells. International Journal of Rock Mechanics and Mining Sciences 40, 1049–1076.